Nanocrystals of $CuCoO_2$ derived from MOFs and their catalytic performance for oxygen evolution reaction

Han Gao,[†,a] Xing Liu,[†,a] Na Han,[b] Lifen Shi,[b] Liang Wang,[a] Yue Mi,[a] Xiao-Qing Bao,[c] Jilin Bai,[a] Hong Li [a] and Dehua Xiong[*,a,b]*

a. State Key Laboratory of Silicate Materials for Architectures, Wuhan University of Technology, Wuhan 430070, P. R. China.

b. State Key Laboratory of Advanced Technology for Float Glass, CNBM Research Institute for Advanced Glass Materials Group Co., Ltd., Bengbu 233017, P. R. China.

c. State Key Laboratory of Optical Technologies on Nanofabrication and Microengineering, Institute of Optics and Electronics, Chinese Academy of Sciences, Chengdu 610209, P. R. China.

* Corresponding author email: xiongdehua2010@gmail.com.

† Han G. and Xing L. contributed equally.

Experimental details

Materials synthesis

The chemicals in these experiments were analytical grade products purchased from sigma Aldrich without further processing. In this experiment, two routes were used to synthesize MOFs derived $CuCoO_2$ (CCO). The first route uses Cu-BTC as the Cu source, $Co(NO_3)$ $6H_2O$ as the Co source, and NaOH as the mineralizer, which are successively dissolved in the mixed solution of ethylene glycol (EG)/isopropanol (IS)/ethanol (ET) and deionized water (DI). Finally, the above solution was put into a 100 ml Taflon-lined autoclave and reacted at different temperatures for 24 hours to obtain Cu-BTC derived CCO (CCO1). In the second route, ZIF-67 was used as the Co source, $Cu(NO_3)_2$ $3H_2O$ as the Cu source, NaOH as a mineralizer, and then dissolved in the mixed solution of ethylene glycol (EG)/methanol (ME)/isopropanol (IS)/ethanol (ET) and deionized water (DI). Finally, the solution was put into a 100 ml Taflon-lined autoclave and reacted at 140 ℃ for 24 hours to obtain ZIF-67 derived $CuCoO_2$ (CCO2) . After the reaction, the obtained CCO1 and CCO2 powders were washed with absolute ethanol and deionized water for several times.

Structural characterizations

The crystal phase of samples was characterized by the powder X-ray diffraction (XRD, D8 Advance). The microstructure, morphology, and composition of as-synthesized MOF-CCO samples were observed using the transmission electron microscopy (TEM, FEI Titan ChemiSTEM operating at 200 keV) coupled with energy-dispersive X-ray spectroscopy (EDS) and the field-emission scanning electron microscopy (FESEM, QUANTA FEG 450) coupled with EDS. The surface chemical states of MOF-CCO powders were analyzed by X-ray photoelectron spectroscopy (XPS, Thermo Escalab 250Xi). XPS measurements were performed at a 01 emission angle using an Al Kα radiator (E_{photon} = 1486.6 eV) with a filament current of 10 mA and a filament voltage energy of 14.7 keV. To compensate for the charging of the sample, a charge neutralizer is used. The C 1s line (284.80 eV) corresponding to the surface adventitious carbon (C-C line bond) has been used as the reference binding

energy. The Brunauer-Emmett-Teller (BET) specific surface areas and porosity parameters of the samples were taken by the N_2 adsorption-desorption isothermetry (Micromeritics TriStar II 3020 3.02). The particle size distribution and average particle size of the sample were determined by Zeta ZS90 & Mastersizer 3000.

Electrode preparation and electrochemical measurement

Firstly, 15.0 mg CCO1 or CCO2 powder was added into a mixture of 500 μL deionized water, 480 μL isopropanol and 20 μL Nafion, and the suspension containing CCO1 or CCO2 powder was obtained by ultrasonic dispersion. The 20.00 μL suspension was dripped on the nickel foam with a working area of 1 x 1 cm^2. Then the electrode was dried (at 150 ℃ for 5 min) for the electrochemical measurements. The loading mass of these electrodes was kept at 0.30 mg cm^{-2}.

The OER performance was evaluated by the cyclic voltammetry (CV) and electrochemical impedance spectroscopy (EIS) in a three-electrode configuration in 1.0 M KOH (pH = 13.5) using a CS2350H electrochemical workstation (Wuhan Corrtest Instruments Corp., China). Presently, the overpotential needed to deliver a benchmark current density of 10 mA cm^2 (η_{10}) is widely employed as an apparent activity indicator for OER electrocatalysts. However, in some cases the oxidation of many transition metal cations from a low valence state to a high valence state overlaps with the OER, and the high catalyst loading could give rise to a large capacitive current (Chem. Commun, 2019, 55, 8744-8763). In this case, assessing and comparing η_{10} (or sometimes η_{10}) based on the polarization curves recorded by positive sweeping of the potential (i.e., comprising the oxidation peak of metal cations) may cause an overestimation in the OER activity (Adv. Mater, 2019, 31, 1806296). Therefore, we propose to present the entire CV curves or negatively swept polarization curves at slow scan rates to minimize the influence of redox peaks and capacitive current. So we chose the CV curves instead of the LSV curves to evaluate the OER activity of CGO based electrodes in this manuscript. A platinum wire and a saturated calomel electrode (SCE) were used as the counter electrode and reference electrode, respectively. The CV scans were recorded between 1.05 and 1.80 V vs.

reversible hydrogen electrode (RHE) at the scan rate of 5 mV s^{-1}. The electrochemical double-layer capacitance (C_{dl}) of each sample was measured given that C_{dl} is positively proportional to the effective surface areas (ESA). C_{dl} can be extracted through CV scans at different rates (from 20 to 100 mV s^{-1}) in the non-faradaic potential window of -0.05 to 0.05 V vs. SCE. The EIS measurements were performed in the frequency range of 20 mHz - 200 kHz under a constant potential of 1.60 V vs. RHE.

All current density values were normalized with respect to the geometrical surface area of the working electrode. All CV curves presented in this work were iR-corrected (85%). The correction was done according to the following equation:

$$E_c = E_m - iR_s, \quad (1)$$

where E_c is the iR-corrected potential, E_m is the experimentally measured potential, and R_s is the equivalent series resistance extracted from the Zero-Input Response (ZIR) measurements. Unless otherwise specified, all potentials were reported versus the RHE by converting the potentials measured vs. SCE according to the following formula:

$$E\ (RHE) = E\ (SCE) + 0.241 + 0.059\ pH \quad (2)$$

Supplementary Tables:

Table S1. Detailed reaction conditions were employed to synthesize Cu-BTC derived delafossite $CuCoO_2$ nanocrystals.

No.	$Co(NO_3)_2$ /g	Cu-BTC /g	NaOH /g	Solvent/mL	Temperature /°C	Time /h
1	0.10	0.10	5.40	2 EG: 70 DI	140	24
2				3 EG: 70 DI		
3				4 EG: 70 DI		
4				50 IS: 20 DI		
5				50 ET: 20 DI		
6			4.40			
7			3.40			
8	0.08		5.40	50 ET: 20 DI		
9	0.06					
10	0.08				120	
11					100	

Table S2. Detailed reaction conditions were employed to synthesize ZIF-67 derived delafossite $CuCoO_2$ nanocrystals.

No.	ZIF-67 /g	$Cu(NO_3)_2$ /g	NaOH /g	Solvent/mL	Temperature /℃	Time /h
1	0.08	0.09	2.96	2 EG: 70 DI	140	24
2				3 EG: 70 DI		
3				4 EG: 70 DI		
4				50 ME: 20 DI		
5				50 ET: 20 DI		
6				50 IS: 20 DI		

Table S3. The OER activity of three electrodes in this work is in comparison to that of other delafossite oxides as well as other perovskite oxides OER catalysts recently reported in the literature.

electrodes	η_{on}/mV	η_{10}/mV	η_{20}/mV	Tafel slope (mV dec^{-1})	C_{dl} (mF cm^{-2})	R_{ct} (Ω)	Ref.
bare Ni	362.2	473.2	510.1	118.0	1.3	17.4	This work
Ni@CCO1	324.3	407.6	438.5	91.3	1.7	5.7	
Ni@CCO2	299.2	394.5	419.3	82.6	2.7	4.6	
GC@$AgCoO_2$	-	395	-	-	-	-	16
Ni@$CuScO_2$	-	470	510	114	-	-	15
GC@CuCoO2	390	440	-	92.8	2.5	65.4	11
GC@$CuCoO_2$	320	390	410	70	6.6	2.9	12
Ni@$CuCoO_2$	375	470	-	96.5	7.0	1.09	17
GC@$LaFeO_3$	360	420	-	62	-	-	55
GC@$LaNiO_3$	-	550	-	148	-	-	56
GC@$LaNi_{0.85}Mg_{0.15}O_3$	-	450	-	95	-	-	56
Carbon@$LiNiO_3$	-	460	-	96	-	-	57
GC@$La_{0.9}Sn_{0.1}NiO_{3-\delta}$	-	318.0	-	74.0	-	-	58

Supplementary Figures:

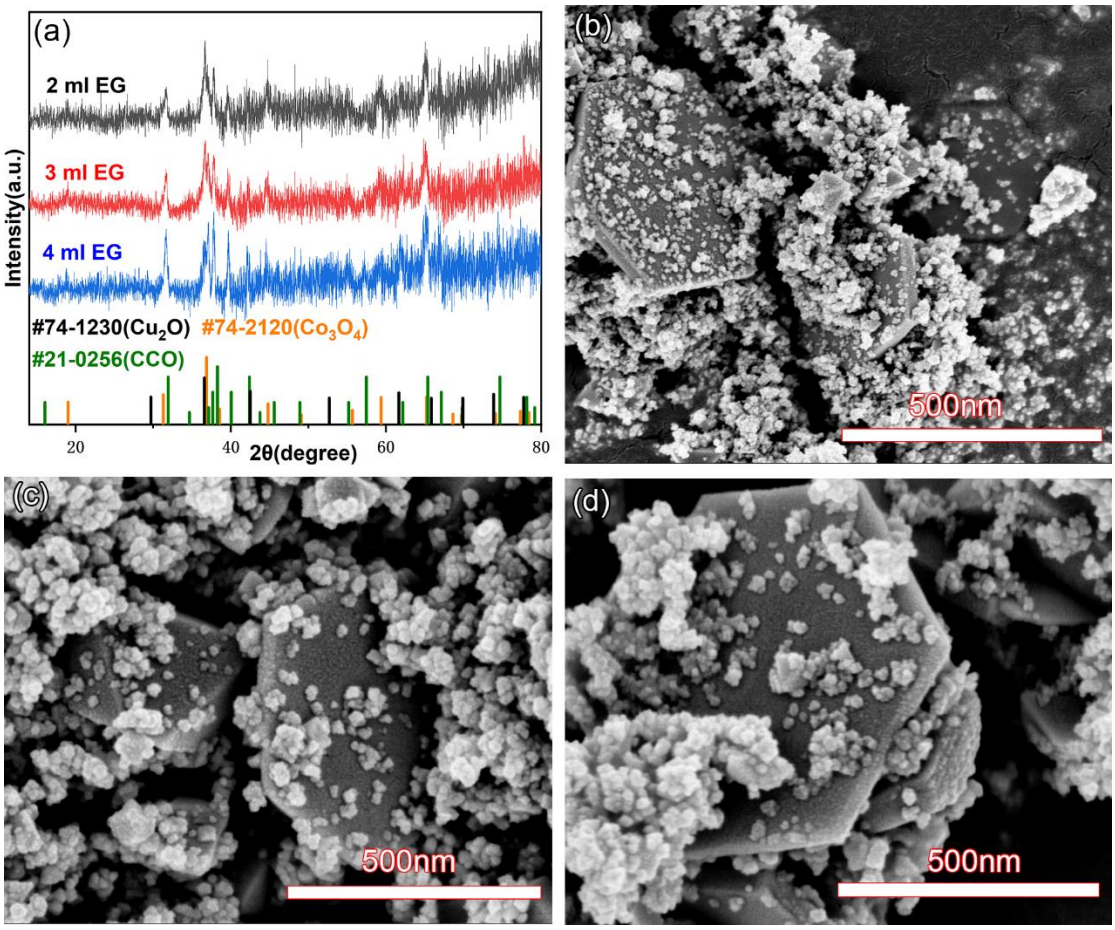

Fig. S1. XRD pattern (a) and SEM images ((b) 2 ml EG, (c) 3 ml EG, (d) 4 ml EG) of the products (samples 1, 2 and 3 in table S1) with different ethylene glycol contents.

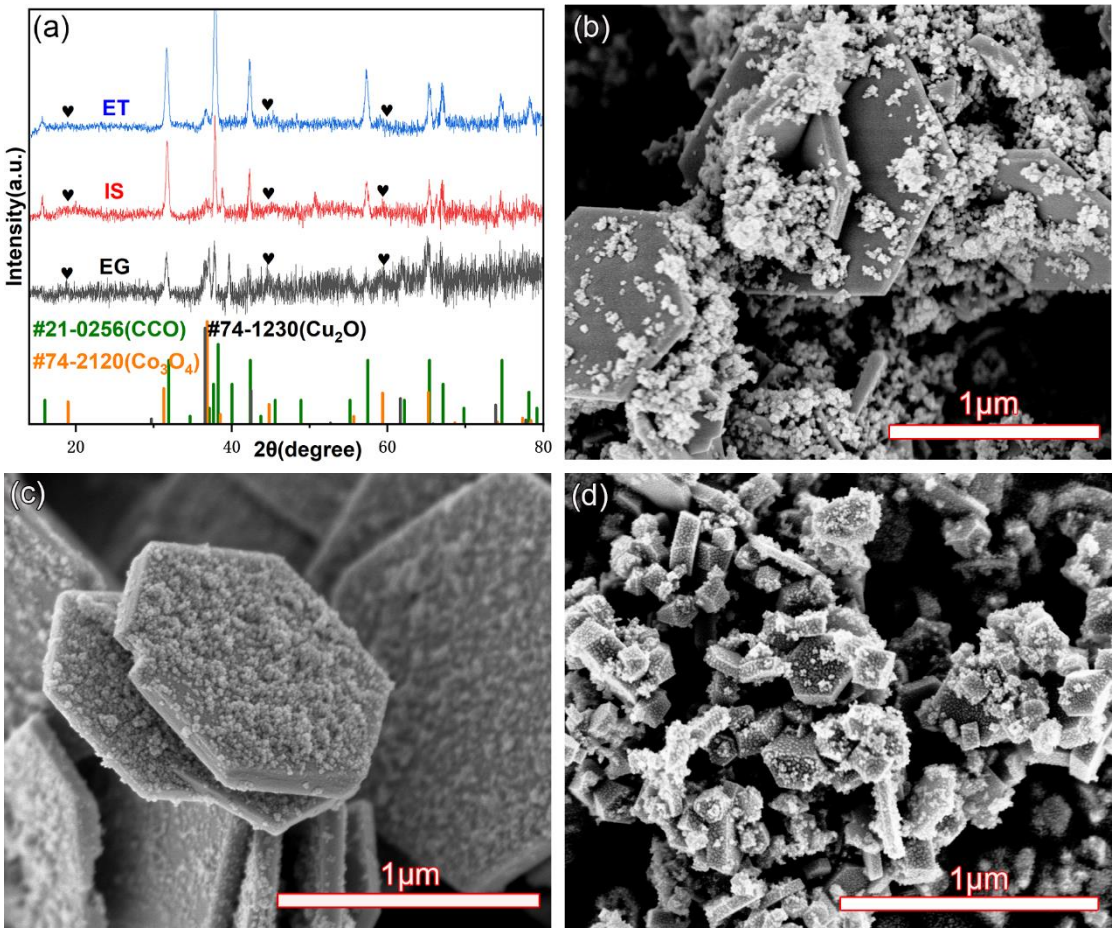

Fig. S2. XRD pattern (a) and SEM images ((b) EG, (c) IS, (d) ET) of products (samples 3, 4 and 5 in table S1) with different reductants.

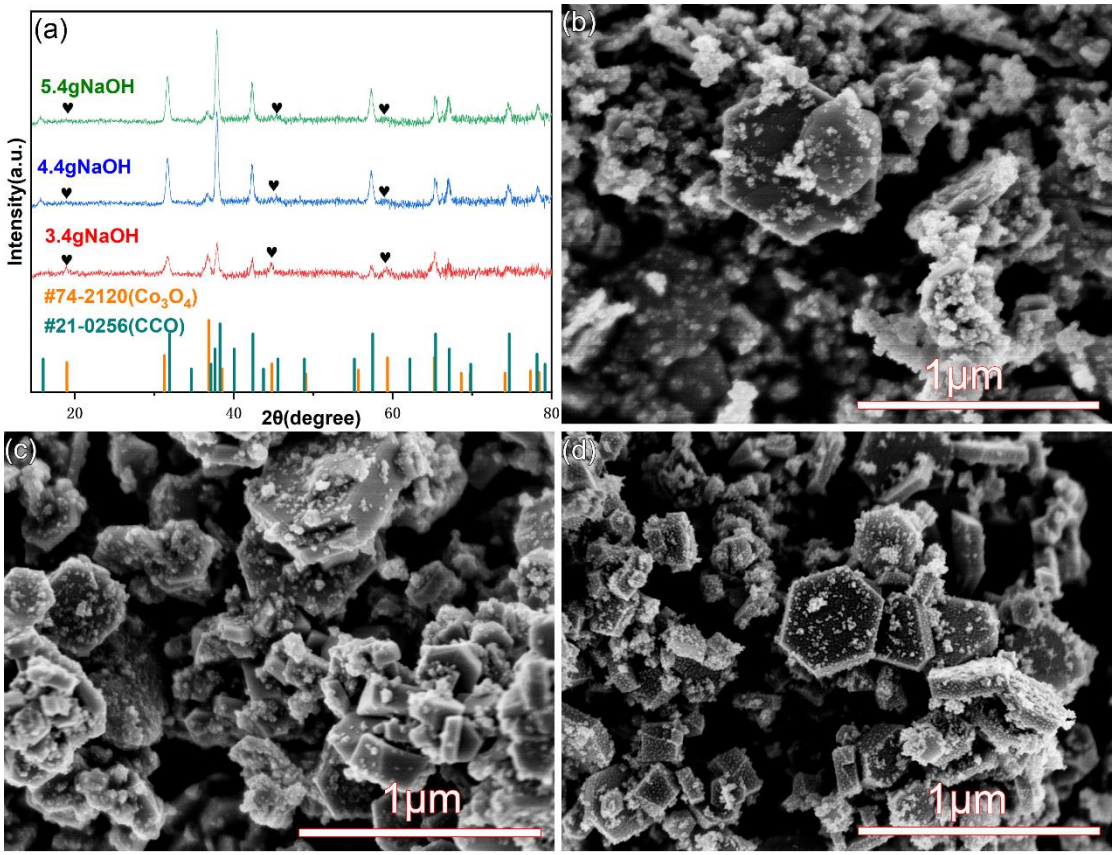

Fig. S3. XRD pattern (a) and SEM images ((b) 3.40 g, (c) 4.40 g, (d) 5.40 g) of products (samples 5, 6 and 7 in table S1) with different amount of NaOH.

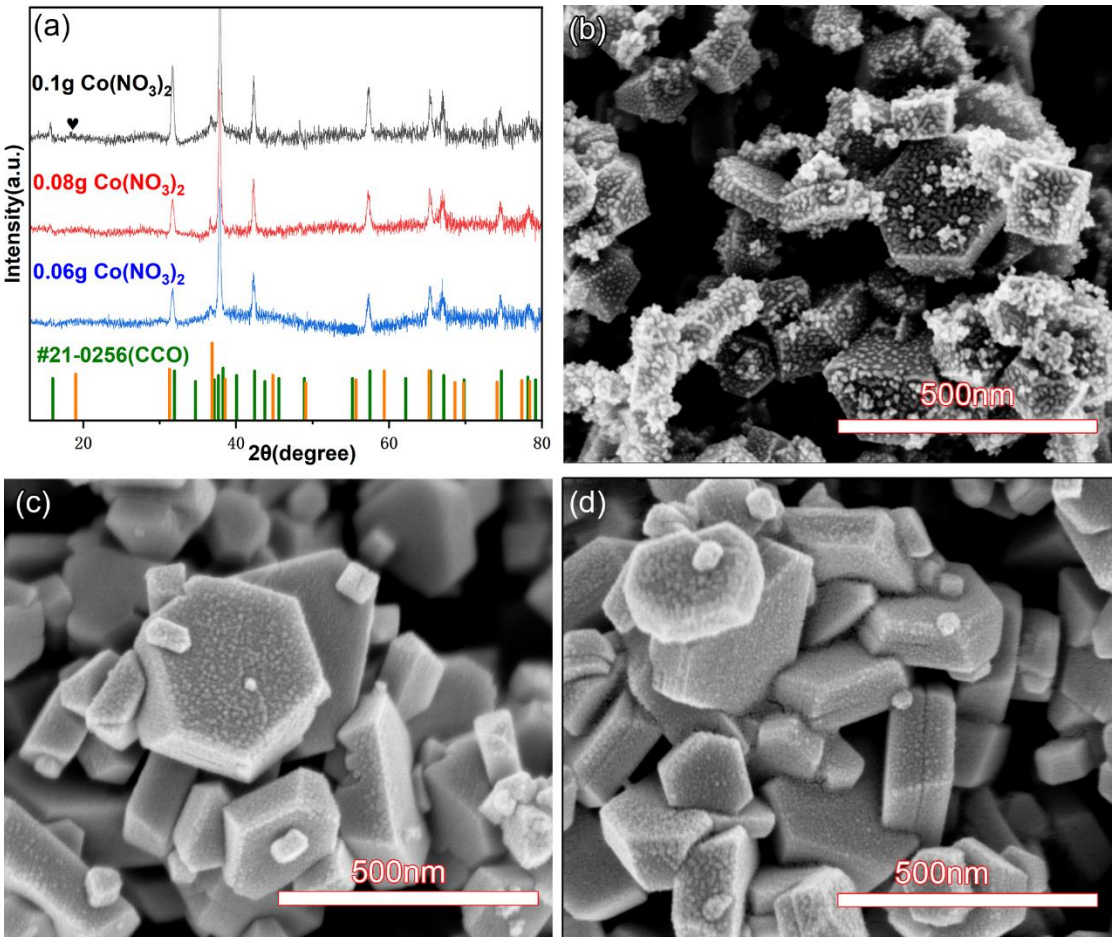

Fig. S4. XRD pattern (a) and SEM images of the products (samples 5, 8 and 9 in table S1) with different $Co(NO_3)_2$ $6H_2O$ addition ((b) 0.10 g, (c) 0.08 g, (d) 0.06 g).

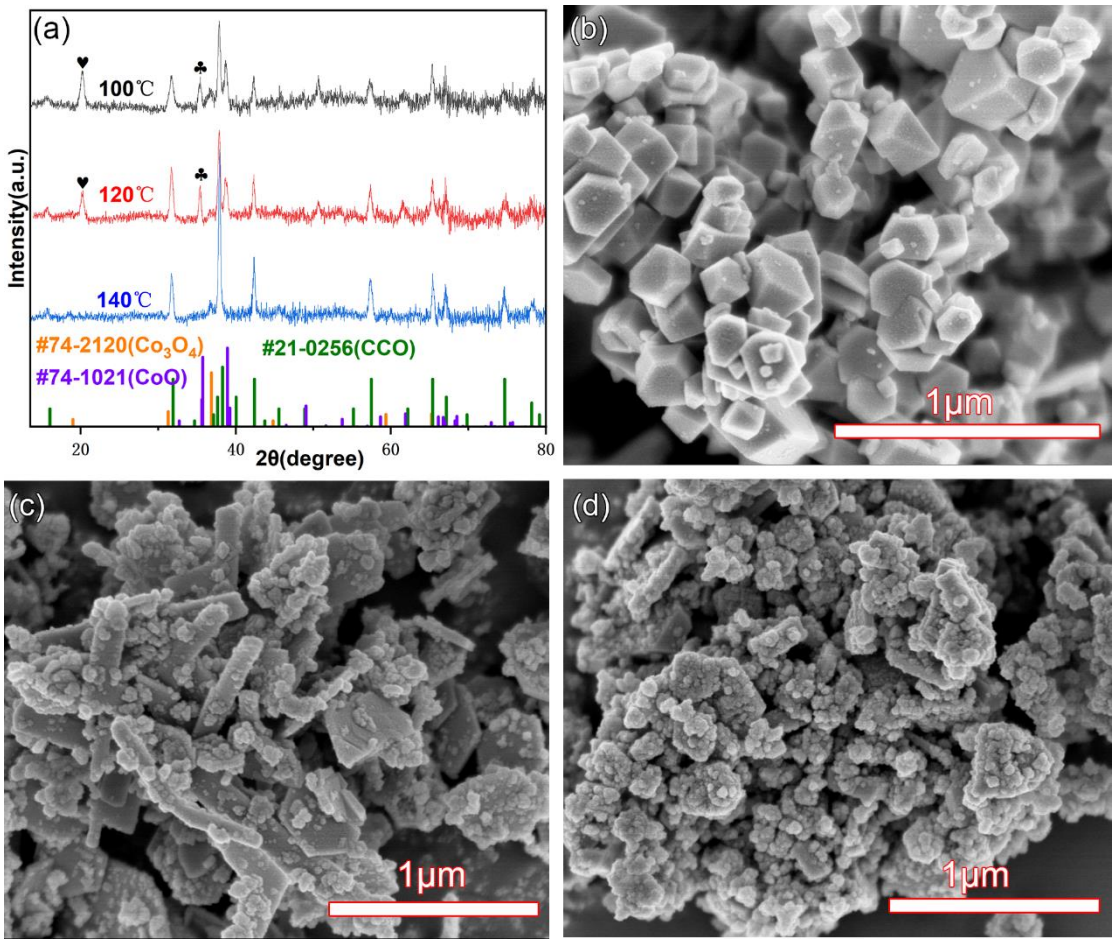

Fig. S5. XRD pattern (a) and SEM images of the products (samples 8, 10 and 11 in table S1) obtained at different reaction temperatures (b, 140 ℃; c, 120 ℃; d, 100 ℃).

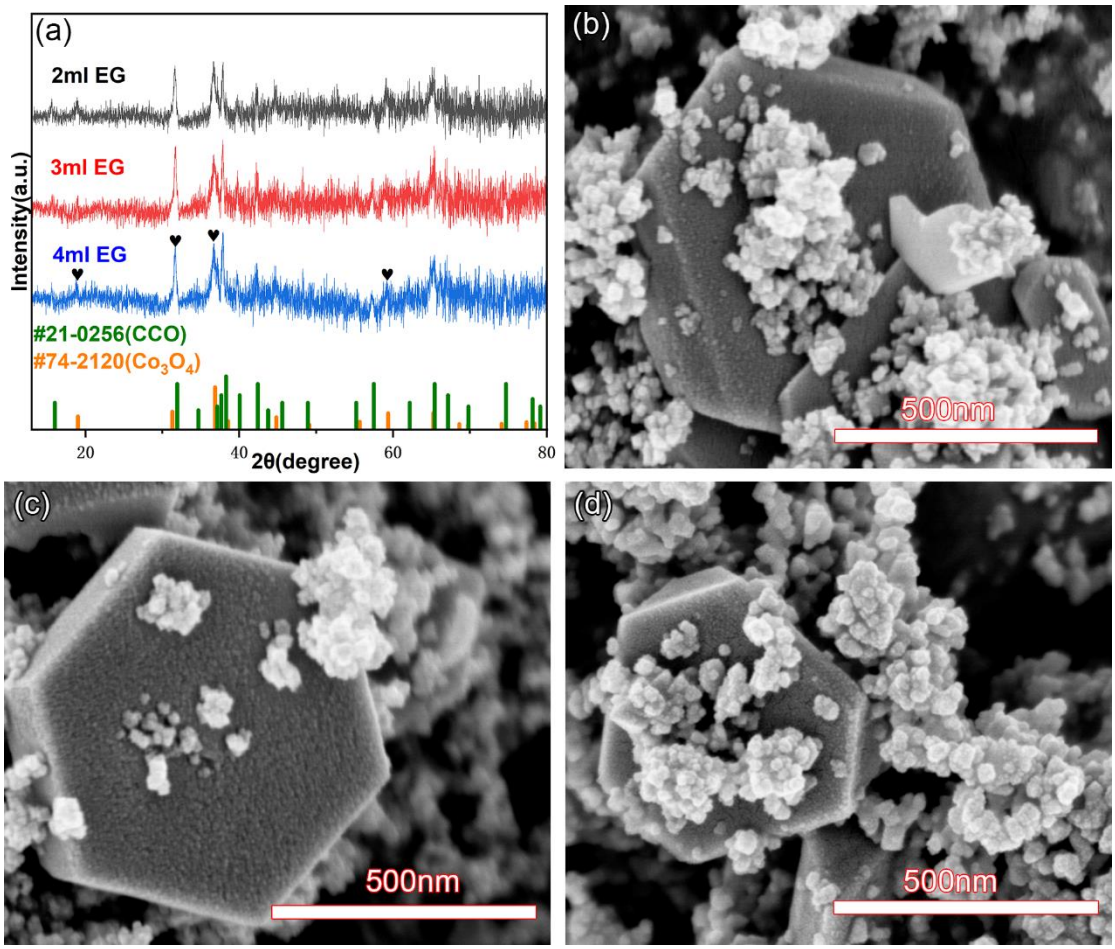

Fig. S6. XRD pattern (a) and SEM images ((b) 2 ml EG, (c) 3 ml EG, (d) 4 ml EG) of the products (samples 1, 2 and 3 in table S2) with different ethylene glycol contents.

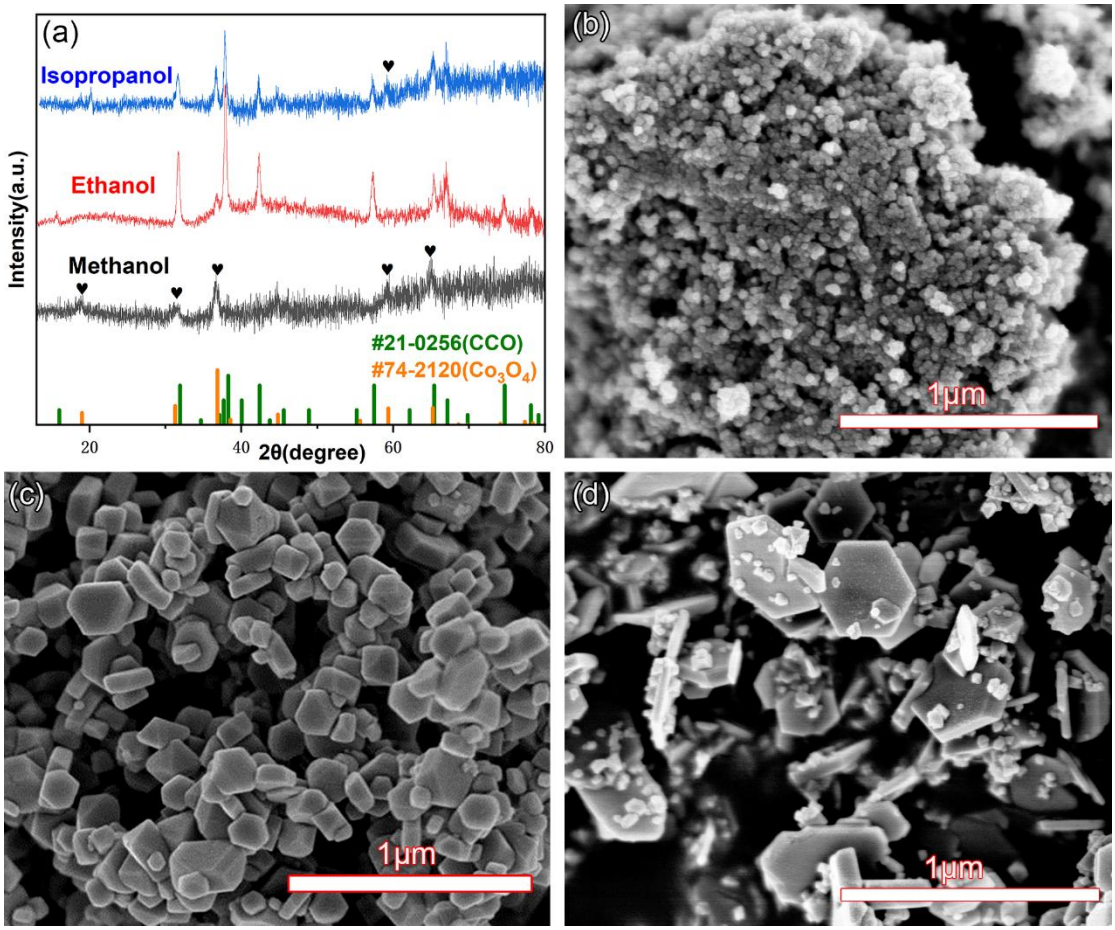

Fig. S7. XRD pattern (a) and SEM images ((b) ME, (c) ET, (d) IS) of products (samples 4, 5 and 6 in table S2) with different reductants.

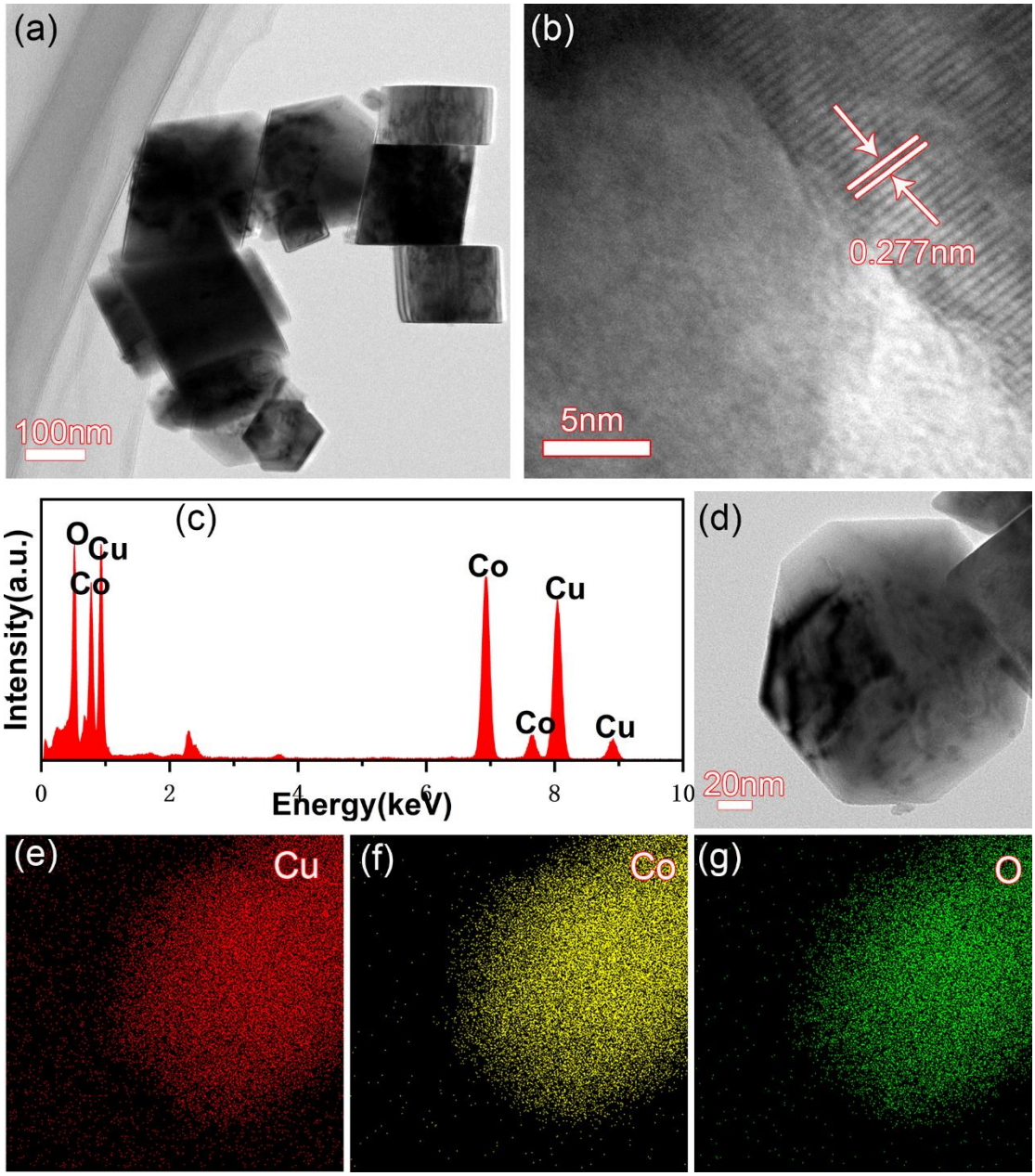

Fig. S8. TEM (a), HRTEM (b), EDS (c), HAADF-STEM (d), and elemental maps (e, Cu; f, Co; g, O) of CCO1.

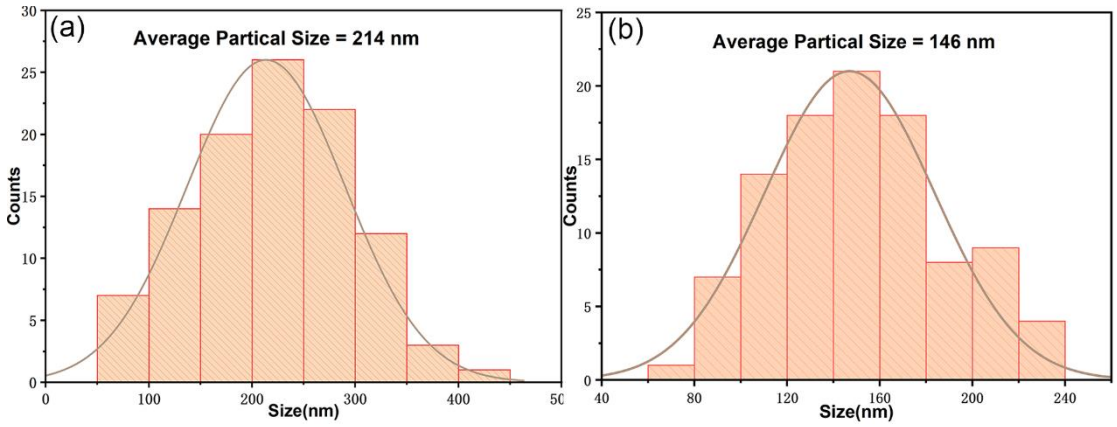

Fig. S9. The partical size distributions of CCO1 (a) and CCO2 (b).

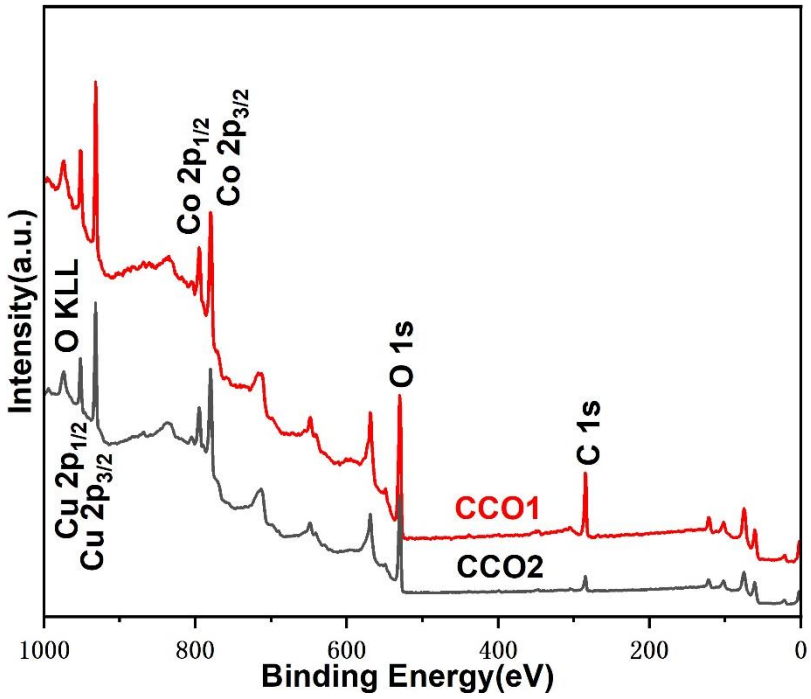

Fig. S10. XPS survey spectrum of CCO1 and CCO2.

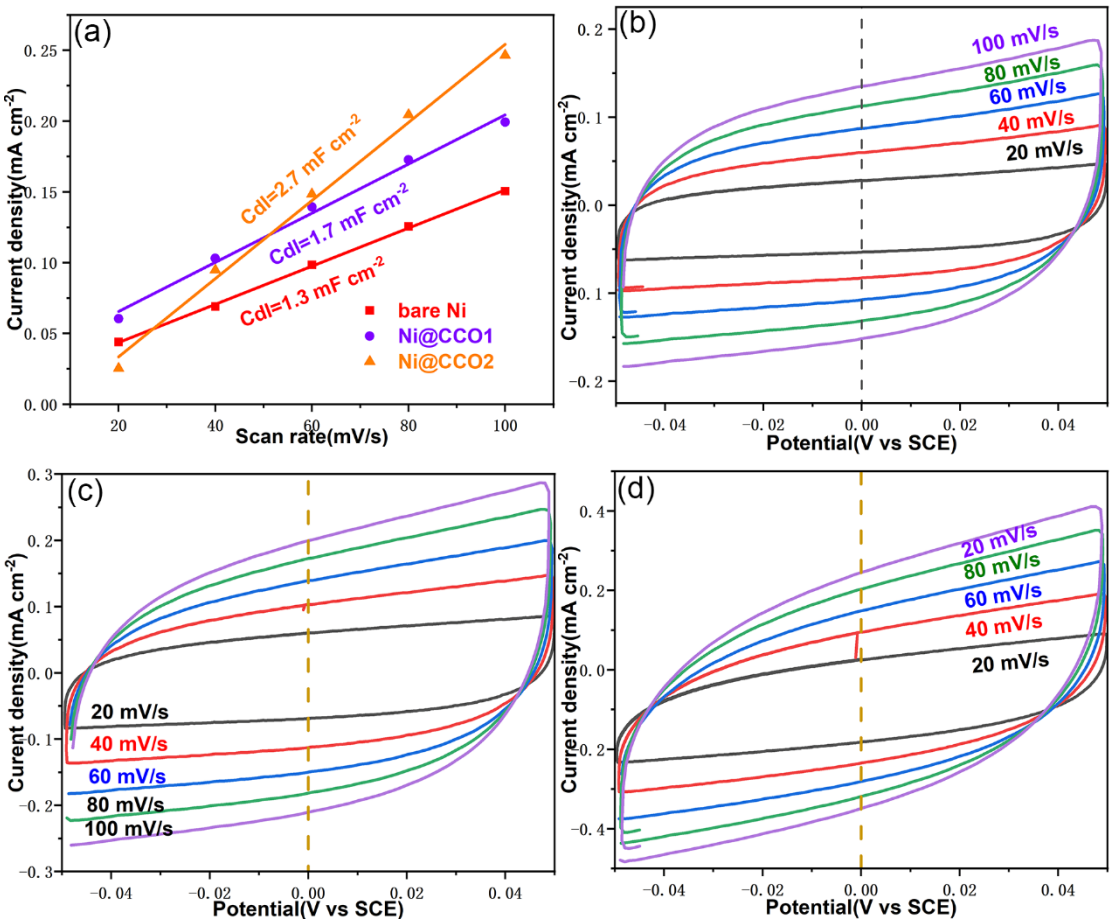

Fig. S11. Double-layer capacitance C_{dl} (a), CV curves at the scan rates from 20 to 100 mV s^{-1} of bare Ni (b), Ni@CCO1 (c), and Ni@CCO2 (d) measured in the non-Faradaic region.

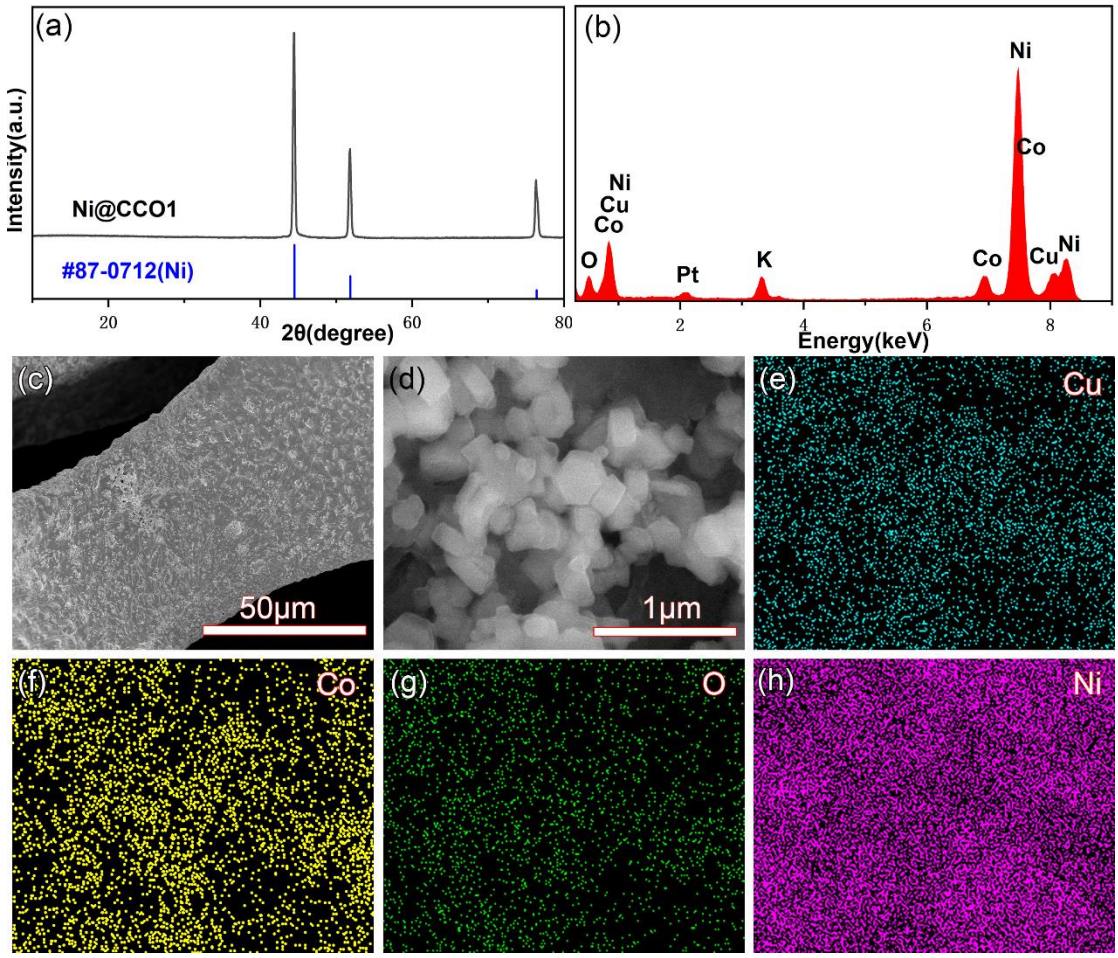

Fig. S12. XRD pattern (a), EDS spectrum (b), SEM images (c, d) and elemental maps (e-h) of Ni@CCO1 after long-term measurement.

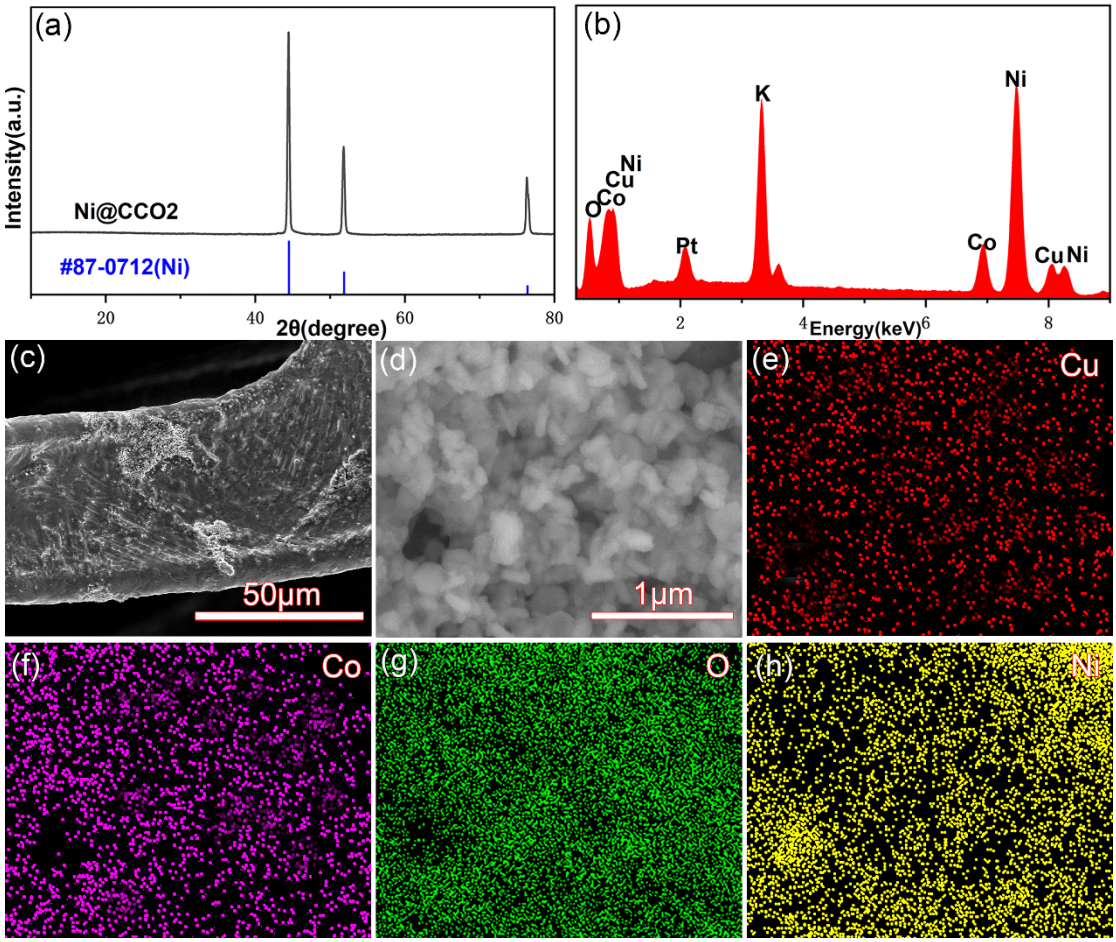

Fig. S13. XRD pattern (a), EDS spectrum (b), SEM images (c, d) and elemental maps (e-h) of Ni@CCO2 after long-term measurement.